Geophysical Research Letters

RESEARCH LETTER
10.1029/2021GL097154

Special Section:
Southern Ocean clouds, aerosols, precipitation and radiation

Extratropical Shortwave Cloud Feedbacks in the Context of the Global Circulation and Hydrological Cycle

Daniel T. McCoy[1], Paul Field[2], Michelle E. Frazer[3,4], Mark D. Zelinka[5], Gregory S. Elsaesser[6,7], Johannes Mülmenstädt[8,9], Ivy Tan[10], Timothy A. Myers[11,12], and Zachary J. Lebo[1]

[1]University of Wyoming, Laramie, WY, USA, [2]United Kingdom Met Office, Exeter, UK, [3]Princeton University, Princeton, NJ, USA, [4]Pennsylvania State University, State College, PA, USA, [5]Lawrence Livermore National Laboratory, Livermore, CA, USA, [6]Department of Applied Physics and Applied Mathematics, Columbia University, New York, NY, USA, [7]NASA Goddard Institute for Space Studies (GISS), New York, NY, USA, [8]Institute for Meteorology, University of Leipzig, Leipzig, Germany, [9]Pacific Northwest National Laboratory, Richland, WA, USA, [10]McGill University, Montreal, QC, USA, [11]Cooperative Institute for Research in Environmental Sciences (CIRES), University of Colorado, Boulder, CO, USA, [12]Physical Science Laboratory, National Oceanic and Atmospheric Administration, Boulder, CO, USA

Abstract Shortwave (SW) cloud feedback (SW_{FB}) is the primary driver of uncertainty in the effective climate sensitivity (ECS) predicted by global climate models (GCMs). ECS for several GCMs participating in the sixth assessment report exceed 5K, above the fifth assessment report "likely" maximum (4.5K) due to extratropical SW_{FB}'s that are more positive than those simulated in the previous generation of GCMs. Here we show that across 57 GCMs Southern Ocean SW_{FB} can be predicted from the sensitivity of column-integrated liquid water mass (LWP) to moisture convergence and to surface temperature. The response of LWP to moisture convergence and the response of albedo to LWP anti-correlate across GCMs. This is because GCMs that simulate a larger response of LWP to moisture convergence tend to have higher mean-state LWPs, which reduces the impact of additional LWP on albedo. Observational constraints suggest a modestly negative Southern Ocean SW_{FB}— inconsistent with extreme ECS.

Plain Language Summary As the climate warms, moisture convergence into the extratropics strengthens, increasing cloudiness, reflected sunlight, and precipitation. Increased cloudiness in response to moisture convergence is affected by how efficiently clouds condense from water vapor relative to how efficiently precipitation depletes them. Simulations where clouds form efficiently cannot reflect much more sunlight in the extratropics because they are already very cloudy and bright. Observations constrain both the sensitivity of reflected sunlight to cloud and of cloud to moisture. Combining these constraints with constraints on other cloud regimes rules out extremely small and large future warming.

Key Points:

- Enhanced moisture convergence with warming creates a negative extratropical cloud feedback
- Cloud source and sink efficiency set the extratropical cloud response
- Constraint by observations suggests a weakly negative feedback- and a moderate effective climate sensitivity

Supporting Information:

Supporting Information may be found in the online version of this article.

Correspondence to:

D. T. McCoy,
daniel.mccoy@uwyo.edu

Citation:

McCoy, D. T., Field, P., Frazer, M. E., Zelinka, M. D., Elsaesser, G. S., Mülmenstädt, J., et al. (2022). Extratropical shortwave cloud feedbacks in the context of the global circulation and hydrological cycle. *Geophysical Research Letters*, *49*, e2021GL097154. https://doi.org/10.1029/2021GL097154

Received 4 DEC 2021
Accepted 17 FEB 2022

1. Introduction

The Shortwave (SW) cloud feedback (SW_{FB}) represents the central uncertainty in the future warming and effective climate sensitivity (ECS) predicted by global climate models (GCMs). Uncertainty in SW_{FB} is a function of the parameterizations of cloud processes necessitated by the relatively coarse resolution of GCMs. Most GCMs transition from a positive SW_{FB} in the subtropics to a negative SW_{FB} poleward of 50°, albeit with substantial uncertainty in magnitude (Gordon & Klein, 2014; Terai et al., 2016; Zelinka et al., 2016, 2020). Several CMIP6 GCMs with very high ECS (>5K) have emerged owing to a more positive extratropical SW_{FB} (Bjordal et al., 2020; Frey & Kay, 2018; Zelinka et al., 2020) and this feature needs to be evaluated.

Different mechanisms have been put forward to explain negative extratropical SW_{FB}:

1. Replacement of susceptible cloud ice with more reflective liquid (McCoy et al., 2014b; Senior & Mitchell, 1993; Tsushima et al., 2006)
2. Suppression of ice hydrometeor sinks of cloud through reduced glaciation (Ceppi, Hartmann, & Webb, 2016; Field & Heymsfield, 2015; Kay et al., 2014; McCoy et al., 2015; Mülmenstädt et al., 2021; Tan & Storelvmo, 2019; Tsushima et al., 2006)
3. Enhanced air-sea exchange of aerosol precursors (Bodas-Salcedo et al., 2019)

4. Strongly increasing adiabatic water content at cold temperatures (Betts & Harshvardhan, 1987; Frazer & Ming, 2022; Terai et al., 2019)
5. Increased extratropical moisture convergence driving enhanced condensation (McCoy et al., 2019, 2020)

We focus on the last of these processes. This is motivated by previous studies that found that changes in surface temperature (T_{skin}) and moisture convergence could be used to explain changes in extratropical cloudiness with minor contributions from other terms such as boundary layer stability and subsidence (McCoy et al., 2020).

It is difficult to untangle the effects of increased local T_{skin} on clouds as it may act through several of the processes listed above. One probable explanation is that increased T_{skin} acts to enhance buoyancy fluxes in the boundary layer, reducing cloud condensate (Bretherton & Blossey, 2014). This mechanism has been found to be important to boundary layer cloud changes across the subtropics (Klein et al., 2017; Myers & Norris, 2016; Myers et al., 2021). Here we treat T_{skin} variations as a proxy for all processes not related to moisture convergence, such as inversion strength as well as other boundary layer processes (Terai et al., 2016, 2019).

SW_{FB} is essentially the change in upwelling SW ($SW_{\uparrow}$) due to clouds scaled by global mean temperature (GMT). $SW_{\uparrow}$ scales with albedo (α) at constant downwelling shortwave radiation and so the proportionality

$$SW_{FB} \propto \frac{d\overline{\alpha}}{dGMT} \sim \frac{\partial \alpha}{\partial LWP} \cdot \frac{d\overline{LWP}}{dGMT} \quad (1)$$

can be used to understand the effects of LWP changes on albedo and shortwave radiation. On the right hand side, the response of $\overline{\alpha}$ to GMT can be broken into the response of α to liquid water mass (LWP) and the response of $\overline{LWP}$ to GMT. As discussed below, overbars denote regional means. The sensitivity $\partial\alpha/\partial$LWP is calculated at the native model resolution as discussed in Section 3.2. The proportionality above only considers the sensitivity of albedo to liquid whereas variations in ice are neglected. This is also discussed in detail in Section 3.2. We investigate and constrain GCM uncertainty in SW_{FB} using terms on the right hand side of Equation 1.

2. Materials and Methods

Section 2.1 discussed the GCM data used in our analysis and Section 2.2 discusses the observational data used to constrain GCM behavior.

2.1. GCM Analysis

The GCM variables examined are clivi (ice water path), clwvi (total cloud water path), pr (precipitation), hfls (evaporative flux at the surface), rsut ($SW_{\uparrow}$ at the top of atmosphere), rsutcs (clear-sky $SW_{\uparrow}$ at the top of atmosphere), ts (T_{skin}), and tas (2m air temperature). clwvi is the sum of IWP and LWP and like microwave LWP is all-sky (averaged over cloudy and clear scenes). We calculate LWP as clwvi-clivi. Precipitation and evaporation are given in units of Wm^{-2}.

For each GCM we analyze the pre-industrial control (piControl) and CO_2 quadrupling (abrupt4xCO2) simulations. The list of analyzed GCMs is given in the supplementary material (Table S1 in Supporting Information S1). The first 150 years of each simulation are examined, consistent with Sherwood et al. (2020).

The latitude range is 40–85°S unless otherwise stated. This is set by the region where zonal precipitation and evaporation difference ($P - E$) is consistently positive, which is similar across GCMs (Figure S1 in Supporting Information S1). $P - E$ approximates moisture convergence when averaged over a large enough region (Held & Soden, 2006).

Our analysis is motivated in part by what variables can be well-observed in the extratropics. LWP is defined as the vertically-integrated mass of cloud liquid in a model grid cell, with the cloud-free portion of the box taken into account in the grid cell average, thus ensuring consistency with microwave observations of LWP (Elsaesser et al., 2017). Microwave LWP is insensitive to multi-layered clouds and does not have any dependence on sun-angle, making it optimal for observing clouds in the extratropics.

Cloud source processes are investigated in the HadGEM3 GCM by perturbing the cloud fraction scheme. HadGEM3 is as described in Mulcahy et al. (2018) and is run in atmosphere-only mode (the General Atmosphere

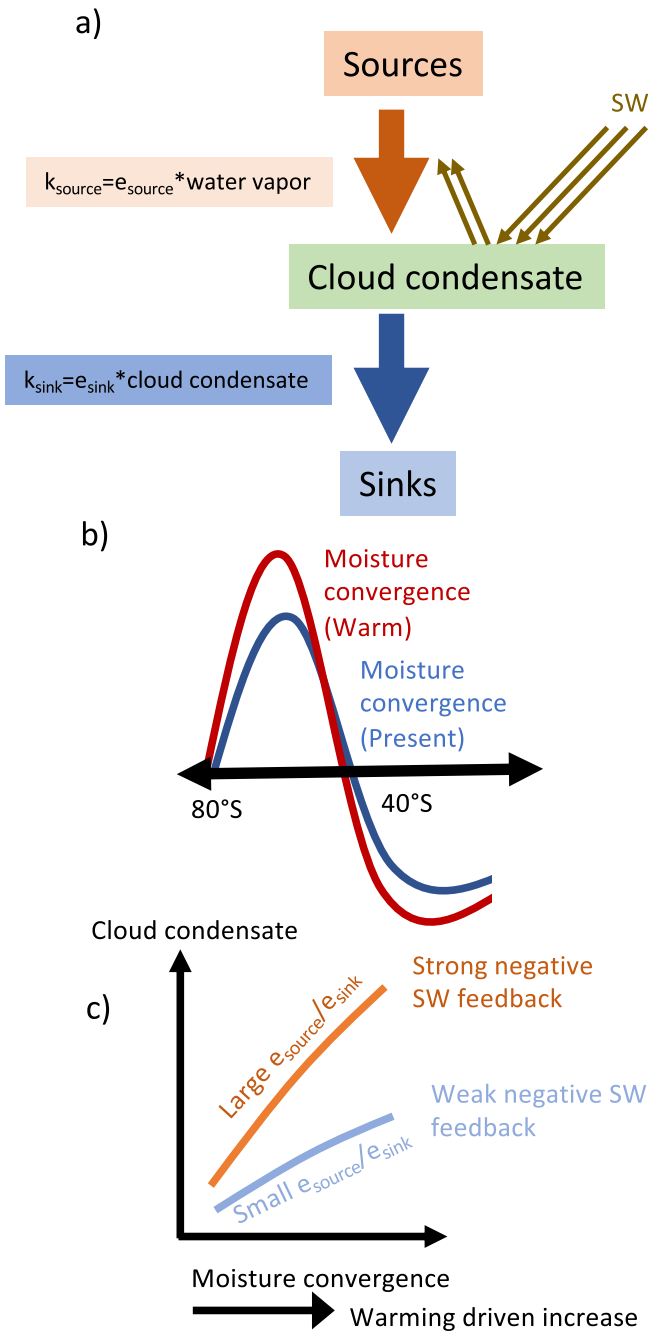

Figure 1. A schematic representation of the moisture convergence-cloud feedback mechanism examined in this study. (a) shows a hypothesized steady-state balance between sources and sinks of cloud. The rate of cloud creation is represented as k_{source}, which is conceptualized as an aggregate efficiency of cloud creation (e_{source}) multiplied by the reservoir of water vapor. The sink term k_{sink} is represented as a bulk sink efficiency (e_{sink}) multiplied by the reservoir of condensed water. (b) shows a cartoon of enhanced moisture convergence (approximated as $P-E$ in the text) in mean-state and warmed climate scenarios due to local and subtropical sources. Finally, (c) illustrates the resulting cloud condensate response to moisture convergence in the context of SW_{FB}. In GCMs where source efficiency is high relative to sinks the increase in LWP will be large resulting in a strongly negative SW_{FB}.

7.1, GA7.1). The only change from the base version of the model is to switch the cloud scheme from PC2 (Wilson et al., 2008) to Smith (1990) because only one parameter needs to be perturbed in the latter.

2.2. Observations

MERRA-2 reanalysis (Molod et al., 2015) is used to characterize mean-state variability in $P-E$, T_{skin}, and 2m temperature. Observations of clear- and all-sky SW flux are taken from the CERES EBAF data set (Ed 4.1) for the period 2000–2016 (Loeb et al., 2018; Wielicki et al., 1996). Observations of LWP are taken from MAC-LWP 1988–2016 (Elsaesser et al., 2017). MAC-LWP is a multi-satellite microwave column LWP record that is corrected for diurnal cycle artifacts and is directly comparable to GCM output without a satellite simulator (Bodas-Salcedo et al., 2011). However, microwave LWP is only available over open ocean (not over sea ice or land). The GCM output used in the main text are not filtered to remove land and sea ice to compare to existing SW_{FB} calculations (Zelinka et al., 2020). Resultant sampling uncertainty is evaluated below.

3. Results

At a regional scale the extratropics are characterized by convergence of moisture carried from the subtropics by transient eddies (e.g., extratropical cyclones) (Algarra et al., 2020; Guo et al., 2020; Hartmann, 2015; Held & Soden, 2006; Yettella & Kay, 2017). As shown in Held and Soden (2006), global warming drives enhanced moisture convergence in this region. Moisture convergence is represented, as in previous work, as $P-E$. As in McCoy et al. (2020), we consider a steady-state model of the extratropical atmosphere. In this framework increased moisture convergence is balanced by increased precipitation. The conversion of vapor to precipitation happens in clouds and increased moisture convergence drives increased cloudiness. This is shown schematically in Figure 1. In this framework the diversity of model responses is driven by the complexity of parameterizing subgrid-scale condensation and precipitation processes. Rates of creation and removal of cloud are considered in terms of efficiency of cloud sources (e_{source}) and sinks (e_{sink}) and the reservoirs of vapor and condensed water (Figure 1a). Global warming causes increased extratropical moisture convergence (Figure 1b). In models where sources are efficient relative to sinks this leads to sharp increases in cloud and a relatively strong negative cloud feedback. If the efficiencies are reversed the negative cloud feedback is weak (Figure 1c; McCoy et al., 2020).

3.1. Changes in Liquid Cloud

In this section we characterize the dependence of extratropical liquid water path ($\overline{LWP}$) on moisture convergence ($\overline{P-E}$) and surface temperature ($\overline{T_{Skin}}$) to predict $d\overline{LWP}/dGMT$ (Equation 1) (Note average of quantities over 40°–85°S are denoted $\overline{(\,)}$.) GCMs predictions of $\overline{LWP}$ vary by an order of magnitude (Figure S2 in Supporting Information S1), while $\overline{P-E}$ varies by only a factor of three (Figure S1 in Supporting Information S1).

As discussed in Section 2.2, LWP is column-integrated all-sky liquid mass, in contrast to focusing on low-topped clouds (Myers et al., 2021). This allows comparison between GCM output and microwave radiometer observations (Elsaesser et al., 2017).

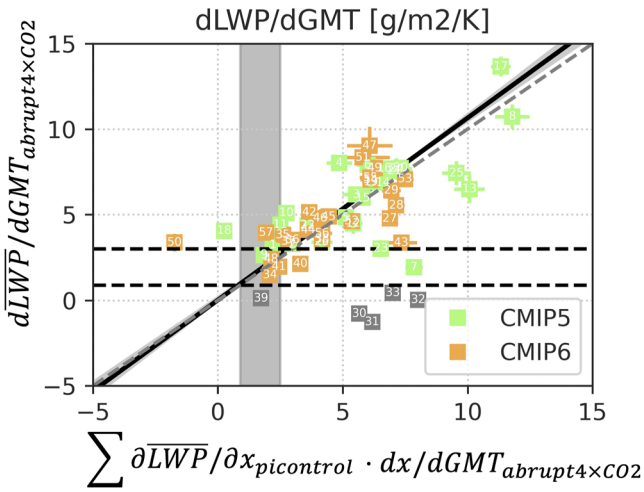

Figure 2. Prediction of the change in extratropical (40–85°S) $\overline{LWP}$ during CO_2 quadrupling from Equation 2. LWP response is normalized by GMT change. The best fit line is shown in black with uncertainty in the best fit in gray shading. The 1-1 line is shown in dashes. Gray markers are not used in the fit (see text for details). The observational constraint is shown as a gray box on the *x*-axis and the intersection with the fit line is shown using horizontal dashed lines.

We choose $\overline{P-E}$ and $\overline{T_{Skin}}$ as cloud controlling factors (Stevens & Brenguier, 2009) based on previous analysis that found that within a given meteorological regime horizontal moisture convergence and sea surface temperature dominated the predicted change in extratropical LWP across a suite of GCMs (McCoy et al., 2019, 2020). The effect of neglecting other predictors in this study will be evaluated by prediction of out-of-sample future simulations, as in Qu et al. (2015). The approximation of moisture convergence as $P-E$ ignores advection out of the atmospheric column and zonal averaging is used to account for zonal advection over the Southern Ocean (Seager & Henderson, 2013).

In each GCM, the multiple linear regression model

$$\overline{LWP} = b_1 \cdot \overline{P-E} + b_2 \cdot \overline{T_{Skin}} + b_3 \quad (2)$$

is trained in the piControl simulation and used to predict the abrupt4xCO2 simulation. This follows the approach used to constrain subtropical cloud feedback in Qu et al. (2015). As discussed in Qu et al. (2015), predictor correlation between cloud controlling factors can be problematic when $R^2 > 0.9$ between predictors. The strongest correlation between predictors in our study was $R^2 = 0.6$.

One of the assumptions inherent to cloud controlling factor predictions is that the relationship between clouds and meteorological factors is unchanged between the climate mean-state and future warmed climates, referred to as "time-scale invariance" (Klein et al., 2017). We evaluate whether the predictors in Equation 2 are time-scale invariant in the context of the GCMs by contrasting coefficients derived in mean-state and warmed simulations as in Qu et al. (2015). The predictors in Equation 2 are consistent when inferred from piControl or from abrupt4xCO2 simulations (Figure S3 in Supporting Information S1).

Equation 2 predicts extratropical LWP. Extratropical moisture convergence is driven by local flux and tropical export (Algarra et al., 2020; Hartmann, 2015). SW_{FB} is typically given as the feedback on global, rather than regional, mean temperature. Thus we write the prediction of LWP response to GMT as:

$$\frac{d\overline{LWP}}{dGMT} = b_1 \cdot \frac{d\overline{P-E}}{dGMT} + b_2 \cdot \frac{d\overline{T_{Skin}}}{dGMT} + b_3 \quad (3)$$

$d\overline{P-E}/dGMT$, and $d\overline{T_{skin}}/dGMT$ are quantified as the linear regression of annual-mean $\overline{P-E}$, and $\overline{T_{skin}}$ on GMT for the first 150 years of abrupt4xCO2. b_{1-3} are calculated using multiple linear regression on monthly-mean piControl output using Equation 2.

The changes in LWP predicted by Equation 3 agree with the abrupt4xCO2 simulations (Figure 2). The correlation between abrupt4xCO2 $d\overline{LWP}/dGMT$ and the prediction based on Equation 3 is $r = 0.71$, and predictions fall along the 1-1 line (see discussion below). Fit lines in Figure 2 are calculated using orthogonal regression with uncertainty in both predictors and predictands. The 95% confidence range on the intercept and slope of the best fit line are calculated using Jackknife resampling (Tukey, 1958). Uncertainty is propagated from uncertainty in b_{1-3} and uncertainty in $d\overline{P-E}/dGMT$ and $d\overline{T_{skin}}/dGMT$.

Several GCMs that share the same cloud physics (CESM2, CESM2-FV, CESM2-WACCM, WACCM-FV, E3SM-1-0) are excluded from the fit in Figure 2. These GCMs are unique in only increasing extratropical LWP in the first 15 years of the abrupt4xCO2 simulation followed by decreasing LWP (Bjordal et al., 2020; Figure S4 in Supporting Information S1). The extratropical cloud response of CESM2 is an active area of investigation at this time and may related to the treatment of ice in the cloud physics parameterization (Bjordal et al., 2020).

An observational constraint on $d\overline{LWP}/dGMT$ is calculated by training Equation 2 on observations from microwave radiometers (Elsaesser et al., 2017) and reanalysis from MERRA-2 (Molod et al., 2015). Observed b_{1-3} (Equation 2, see Figure S3 in Supporting Information S1) is combined with $d\overline{P-E}/dGMT$ and $d\overline{T_{Skin}}/dGMT$

for each GCM following Equation 3. Uncertainty is propagated from uncertainty in b_{1-3}, but is dominated by spread between GCMs in $d\overline{P-E}/dGMT$ and $d\overline{T_{Skin}}/dGMT$.

Microwave LWP is only available over open water (Wentz & Meissner, 2000). We quantify the sampling error due to neglecting data over ice and land. Predicted $d\overline{LWP}/dGMT$ for GCMs when the regression model (Equation 2) is trained using only data over open water is contrasted with the value when all data is used. Monthly values on the native grid of the GCM where $\alpha_{\text{clear-sky}} > 0.4$ are excluded to remove ice and land. The zonal-, latitudinal-, monthly-means calculated from the filtered data are used to train Equation 2. The constraint on $d\overline{LWP}/dGMT$ is not strongly affected by only considering open ocean (Figure S5 in Supporting Information S1) and sampling error is included in the constraint in Figure 2.

The median value and standard deviation of $d\overline{P-E}/dGMT$ across GCMs is 0.77 ± 0.39 $\text{Wm}^{-2}\text{K}^{-1}$. For $d\overline{T_{Skin}}/dGMT$ it is 1.19 ± 0.36 K/K. The relative contribution to $d\overline{LWP}/dGMT$ by changes in $\overline{P-E}$ has a median value of 15% across GCMs but ranges from 0% up to 250% (values greater than 100% occur in GCMs where contributions from surface warming and moistening have opposing effects on $\overline{LWP}$). $\overline{P-E}$ scales at slightly less than implied by Clausius-Clapeyron, which is consistent with earlier studies (Lorenz & DeWeaver, 2007). There is a median increase of 5.3%/K across the GCMs surveyed here.

Combining the observational constraint on $d\overline{LWP}/dGMT$ with the best fit line in Figure 2 yields a constraint on $d\overline{LWP}/dGMT$ ranging from 0.9 to 3.0 · g · $\text{m}^{-2}\text{K}^{-1}$. Direct comparison to other studies is difficult given differing study regions, lack of regime-partitioning, temporal-averaging and configurations of the warming signal, but qualitatively there is agreement regarding an increase in extratropical LWP in response to warming, albeit weaker than most GCMs (Figure S2 in Supporting Information S1) (Ceppi, McCoy, & Hartmann, 2016; Ceppi & Nowack, 2021; Manaster et al., 2017; McCoy et al., 2019, 2020).

Based on our analysis, we find that extratropical LWP changes in response to warming across many GCMs can be predicted based on their present-day, monthly covariability between Southern Ocean LWP, moisture convergence, and T_{Skin}. Given that these terms are among the simplest descriptors of atmospheric state (is the atmosphere warm on the bottom and is it moist), this is not too unexpected.

3.2. Compensation Between Moisture Removal and Radiative Efficiency Across GCMs

We now consider the radiative sensitivity term ∂α/∂LWP from Equation 1. Because LWP integrates over cloudy and clear regions (Elsaesser et al., 2017) it is an emergent property of a complex population of clouds. To first order, the relation between LWP and $\text{SW}_{\uparrow}$ is a function of cloud areal extent (Bender et al., 2017), cloud optical thickness (Gordon & Klein, 2014), and the underlying surface properties (increased cloud will affect $\text{SW}_{\uparrow}$ more over a dark surface). To quantify how $\text{SW}_{\uparrow}$ responds to changes in LWP, we train the following multiple linear regression model relating albedo (α) to LWP and clear-sky α ($\alpha_{\text{clear-sky}}$)

$$\alpha = c_1 \cdot LWP + c_2 \cdot \alpha_{clear-sky} + c_3 \tag{4}$$

where $\alpha = \text{SW}_{\uparrow}/\text{SW}_{\downarrow}$ is calculated from monthly means of top-of-atmosphere flux. (Note the lack of overbars in Equation 4. This is because a regional average is not required as it is in Equation 2 to make $P - E$ a reasonable approximation for moisture convergence.) The regression model in Equation 4 is trained on data from 40° to 85°S at the native resolution of each GCM. It is trained independently in each calendar month due to residual effects from the seasonal cycle of solar zenith angle, which enhances α (McCoy et al., 2018). The regression model in Equation 4 could easily be improved, for instance by including information about IWP (which can be considered to be included in c_3) or information about cloud fraction not already implicitly included in LWP, but we have chosen to consider variables that can be quantified accurately in observations and that are available from GCMs without the use of a satellite simulator (Bodas-Salcedo et al., 2011; Jiang et al., 2012)—in this case LWP and $\text{SW}_{\uparrow}$. LWP changes are generally much larger than IWP in the 40–80°S region with a median ratio of liquid to IWP change across GCMs of 8. Further, ice tends to be less reflective than liquid for a unit mass, (McCoy et al., 2014a) suggesting that neglecting it here does not adversely affect our prediction of albedo change.

The sensitivity of α to LWP (∂α/∂LWP) derived from piControl simulations is inversely related to the mean-state LWP (Figure 3). Albedo and cloud fraction (the areal coverage of cloud, CF) are nearly linearly related (Bender et al., 2017), but the effects of in-cloud LWP ($\text{LWP}_{\text{in-cloud}}$) on α saturates at high $\text{LWP}_{\text{in-cloud}}$ (Lacis &

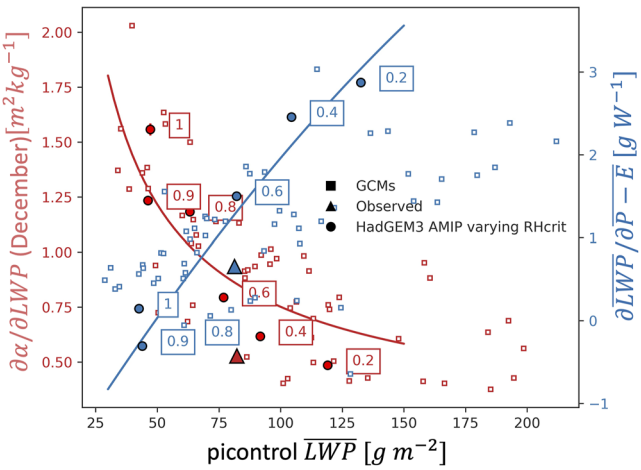

Figure 3. Radiative efficiency ($\partial\alpha/\partial$LWP) and moisture sensitivity ($\partial\overline{LWP}/\partial\overline{P-E}$) anti-correlate across GCMs as a function of mean state extratropical $\overline{LWP}$. Observations from CERES, MERRA-2, and MAC-LWP are shown using triangles. Simulations in HadGEM3 perturbing source strength (RH_{crit} is noted in boxes) are shown as circles. A powerlaw is used to fit $\partial\alpha/\partial$LWP and a second order polynomial is used to fit $\partial\overline{LWP}/\partial\overline{P-E}$.

Hansen, 1974; Liou, 2002). LWP includes information about $LWP_{in-cloud}$ and cloud extent ($LWP \approx CF \cdot LWP_{in-cloud}$); thus, as the LWP across the extratropics increases, liquid begins to affect $SW_{\uparrow}$ less efficiently by increasing liquid water density in cloud rather than filling in cloud cover. This leads to the saturation in $\partial\alpha/\partial LWP$ as a function of increasing mean-state LWP.

Equation 4 is trained on observations from CERES and MAC-LWP to yield an observational estimate of $\partial\alpha/\partial$LWP. The $\partial\alpha/\partial$LWP estimated from observations falls along the relation between mean-state LWP and $\partial\alpha/\partial$LWP emerging from GCMs (Figure 3). This is encouraging as it suggests that the relationship between LWP and α is based on radiative transfer and distributions of cloud that are well-represented in GCMs (time-scale invariance is shown in Figure S3 in Supporting Information S1). $\partial\alpha/\partial$LWP inferred from observations is on the lower end of the $\partial\alpha/\partial$LWP in GCMs. The finding that GCM $SW_{\uparrow}$ is too sensitive to LWP is consistent with previous studies (Kelleher & Grise, 2019).

The sensitivity of LWP to converging moisture ($\partial\overline{LWP}/\partial\overline{P-E}$, Equation 2) correlates positively with mean-state LWP (Figure 3). The sensitivity of LWP to T_{skin} ($\partial\overline{LWP}/\partial\overline{T_{Skin}}$) does not correlate with mean-state LWP, and 95% of GCMs fall between -0.1 g $\cdot$ m^{-2}K^{-1} and 7.0 g $\cdot$ m^{-2}K^{-1}. It is inferred from observations that $\partial\overline{LWP}/\partial\overline{T_{Skin}} = 0.6 \pm 0.1$ g $\cdot$ m^{-2}K^{-1}. The diagnosed relationship relating LWP to T_{skin} is likely to represent several processes (Terai et al., 2019). We focus on $\partial\overline{LWP}/\partial\overline{P-E}$ because of its emergent relationship with mean-state LWP.

The relationship between $\partial\overline{LWP}/\partial\overline{P-E}$ and mean-state $\overline{LWP}$ shown in Figure 3 can be explained in the framework of sources and sinks of cloud (Figure 1). LWP will be high when sources of cloud are efficient relative to sinks. Further, LWP will be sensitive to increased moisture convergence (a large $\partial\overline{LWP}/\partial\overline{P-E}$). However, radiation will be insensitive to increased LWP (a small $\partial\alpha/\partial$LWP) because the extratropics will already be extremely cloudy (CF $\approx$ 1) and thus there will be relatively few clear patches that can be filled in for maximum radiative effect. Instead, overcast regions must increase in-cloud liquid content for diminishing returns in $SW_{\uparrow}$.

We test the hypothesis that the dependence of $\partial\overline{LWP}/\partial\overline{P-E}$ and $\partial\alpha/\partial$LWP on mean-state $\overline{LWP}$ is a function of varying cloud source and sink strength using HadGEM3 run in atmosphere-only mode (Mulcahy et al., 2018) with the Smith cloud scheme (Smith, 1990), which uses a critical relative humidity (RH_{crit}; Quaas, 2012; Smith, 1990). Use of the Smith cloud scheme allows us to represent the strength of the source term using a single parameter (RH_{crit}). RH_{crit} is varied from 100% (clouds are only formed when the GCM grid box has total relative humidity >100%) to 20%. The mean-state pattern of $P-E$ changes dramatically for RH_{crit} <80%. To provide a fair comparison to the coupled GCMs we examine the latitude range in each HadGEM3 simulation where climatological, zonal-mean $P-E$ is positive as opposed to selecting 40–85°S, as in the coupled GCMs (see Figure S1 in Supporting Information S1). The dependence of $\partial\overline{LWP}/\partial\overline{P-E}$ and $\partial\alpha/\partial$LWP on mean-state LWP derived from the HadGEM3 simulations agrees with the behavior of the coupled GCMs. As RH_{crit} decreases (stronger cloud source) $\partial\overline{LWP}/\partial\overline{P-E}$ increases and $\partial\alpha/\partial$LWP decreases. This supports our hypothesis that the relative efficiency of sources and sinks in GCMs affect mean-state cloud, the response of extratropical cloud to increased moisture convergence, and the effect of increased cloud on $SW_{\uparrow}$.

In summary, strong responses of LWP to moisture convergence in warming simulations are compensated by weak increases in $SW_{\uparrow}$ in response to LWP. The relationships in Figure 3 may provide a useful process-level constraint on GCMs.

3.3. Constraints on SW Cloud Feedback

In the preceding sections we provided constraints on the terms on the right-hand-side of Equation 1. We now combine these constraints to provide a constraint on SW_{FB} following Equation 1. It is found that Equation 1 using values from Figures 2 and 3 predicts SW_{FB} across GCMs (Figure 4a). The term $\partial\alpha/\partial$LWP is calculated via Equation 4 using December values (when insolation is strong).

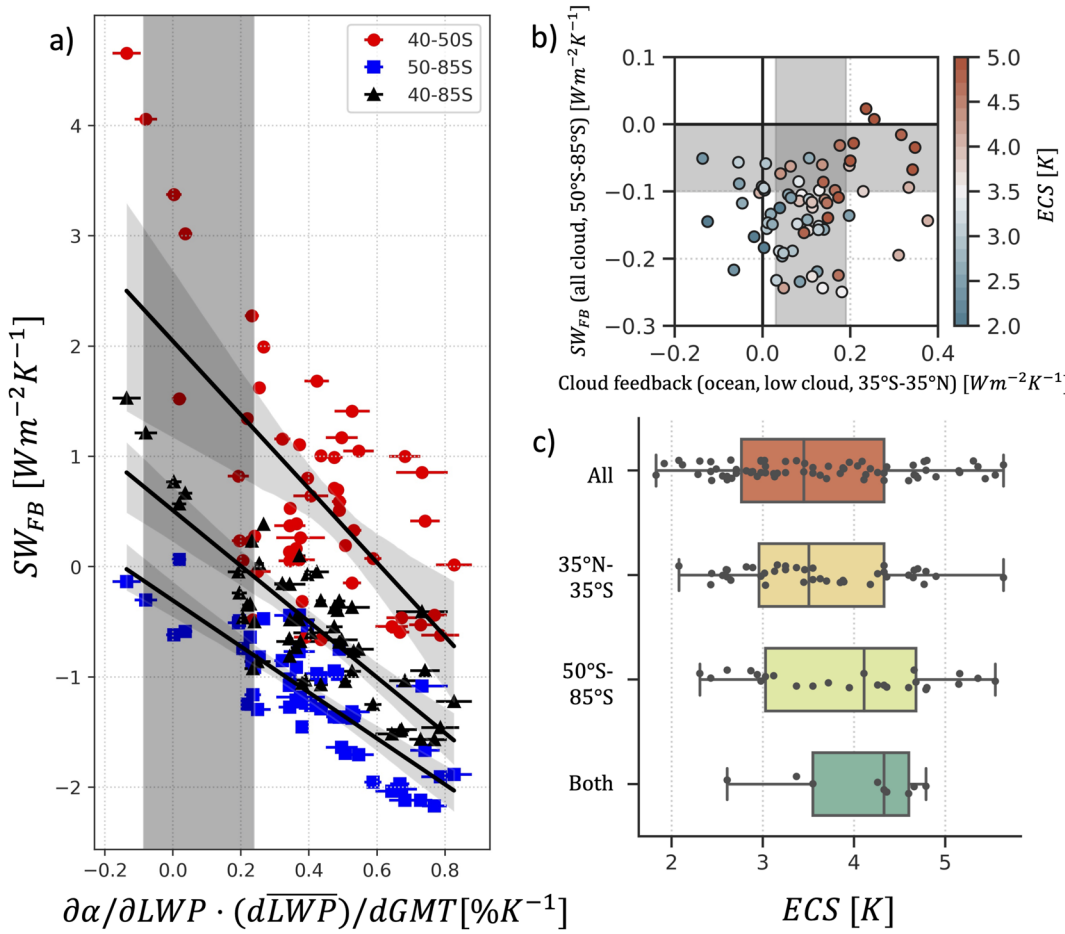

Figure 4. (a) SW cloud feedback (SW_{FB}) as a function of the predicted response of 40–85°S $\overline{LWP}$ to GMT ($d\overline{LWP}/dGMT$, Figure 2) scaled by the sensitivity of α to LWP ($\partial\alpha/\partial$LWP, Figure 3). The range consistent with observations is shown as a shaded gray box and the best fit regression and 95% confidence on the fit are shown using a black line and gray shading. SW_{FB} is shown averaged over three regions: 40–50°S (drying driven by Hadley cell expansion), 50–85°S (the region of consistent moistening), and 40–85°S. (b) the distribution of 50–85°S SW_{FB} and 35°S–35°N total marine low cloud feedback in CMIP5 and CMIP6 GCMs colored by ECS. Observational constraints from this study (*y*-axis, panel (a)) and consistent with Myers et al. (2021) (*x*-axis) are shown as gray shading (Text S1 in Supporting Information S1). SW_{FB} is shown weighted by global surface area-in contrast to (a). (c) the effects on the distribution of ECS in CMIP5 and CMIP6 of removing GCMs not consistent with the constraints shown in (b). The effect of constraining the prior distribution of models by subtropical and extratropical constraints from (b) are shown along with the result of applying both constraints at once.

The prediction of SW_{FB} for three regions by 40–85°S $d\overline{LWP}/dGMT$ and $\partial\alpha/\partial$LWP is shown. Moistening is not uniform across the 40°–85°S region (Figure S1 in Supporting Information S1). LWP is reduced in the 40°–50°S region consistent with Hadley cell expansion and drying (Grise & Medeiros, 2016; Kay et al., 2014; Kelleher & Grise, 2021; Lu et al., 2007; Sousa et al., 2018; Tselioudis et al., 2016; Figure S1 in Supporting Information S1) and SW_{FB} tends to be positive in this region (Figure 4a). In the 50–85° S region there is consistent moistening (Figure S1 in Supporting Information S1), LWP increases (Figure S2 in Supporting Information S1), and SW_{FB} tends to be negative (Figure 4a). The prediction of SW_{FB} averaged 40°–85°S is the area-weighted sum of these effects. Clearly, influence on the region of moistening by Hadley cell expansion modulates extratropical SW_{FB} (Kelleher & Grise, 2021).

Prediction of Hadley cell expansion is beyond the scope of this work. Thus, we examine the region of consistent moistening. Equation 1 explains 83% of the variance in SW_{FB} averaged between 50° and 85°S (Figure 4a). The observational constraints on the right hand side of Equation 1 predicts the contribution to global-mean SW_{FB} from the 50°–85°S region to be between −0.1 $Wm^{-2}K^{-1}$ and 0.0 $Wm^{-2}K^{-1}$, consistent with the interpretation of

Equation 1 as an emergent constraint on 50°–85°S SW_{FB} (Hall & Qu, 2006; Klein & Hall, 2015). In summary, SW_{FB} is negative in regions of moistening.

3.4. Conclusion and Probable Range of ECS

How does the constraint on SW_{FB} from Equation 1 inform the most probable range for ECS? For illustrative purposes we detail a simple constraint. The ECS calculated from 71 CMIP5 and CMIP6 models (Zelinka et al., 2020) is constrained by 50°–85°S (extratropical moistening regime) and 35°S–35°N (subtropical) cloud feedback (Figure 4b). The subtropical marine, low-topped cloud feedback is examined for consistency with previous studies (Myers et al., 2021; Text S1 in Supporting Information S1). The number of GCMs is increased here because fewer GCMs have all the necessary variables to examine moisture and cloud changes, as detailed in the preceding sections. The subtropical and extratropical SW_{FB} are considered simultaneously because subtropical cloud feedback is a key uncertainty (Bony, 2005; Bretherton & Caldwell, 2020; Myers & Norris, 2016).

More positive cloud feedback in either averaging region corresponds to higher ECS. Subtropical and extratropical cloud feedbacks are correlated across GCMs (Figure 4b). Constraining GCMs to be consistent with constraints on either regional cloud feedback doesn't substantially narrow ECS (Figure 4c). Consideration of both constraints results in ECS falling between 2.6 and 4.8 K with a median of 4.3 K. No GCMs with ECS <2.5K or >5K out of the original 71 GCMs are consistent with constraints on both subtropical and extratropical cloud feedback and the means differ at 95% confidence using a Welch's *t*-test. However, this approach is sensitive to the prior distribution from GCMs.

We calculate a more rigorous constraint on ECS using the World Climate Research Programme (WCRP) Bayesian framework (Sherwood et al., 2020). In Sherwood et al. (2020) process-level understanding of cloud feedbacks from the literature was evaluated and the most likely ranges for cloud feedback in various geographic regions and cloud regimes were input into a Bayesian model along with other constraints on ECS, such as paleoclimate records. The cloud feedbacks in the 50°–85° regions considered by Sherwood et al. (2020) were: 40°–70° cloud optical depth set at 0.0 $Wm^{-2}K^{-1} \pm 0.2$ at 95% confidence and middle latitude (30°–60°) marine low cloud set at $+0.08 \pm 0.16$ $Wm^{-2}K^{-1}$. All other potential cloud feedbacks in the 50°–85° region were assumed to be 0.0 ± 0.0 Wm^{-2} K^{-1} because of insufficient process-level understanding and constraints.

Summing the different probable feedback values from Sherwood et al. (2020) for the 50°S–85°S region (assuming all feedbacks are constant in their given latitude ranges) gives a value of $+0.01 \pm 0.06$ Wm^{-2} K^{-1}. Both Sherwood et al. (2020) and Figure 4 suggest very negative extratropical cloud feedbacks are unlikely. However, we can infer from Figure 4 that the most likely value of SW_{FB} to be negative because it does not neglect non-boundary layer cloud, or cloud poleward of 70°, for which GCMs consistently predict a negative SW_{FB} (Ceppi, McCoy, & Hartmann, 2016; Terai et al., 2016; Zelinka et al., 2016).

The latitude range used in the WCRP assessment for the extratropical region (oceans 60°–90° in both hemispheres) differs slightly from our analysis of the uniform moistening in the Southern Ocean (50°–85°S). To use the existing WCRP code we need to offer a prediction for the 60°–90° oceans. Using the predictor in Figure 4 for 60°–90° yields a similar prediction (Figure S6 in Supporting Information S1) to those shown in Figure 4a. Combining this value with the constraint provided by Myers et al. (2021) results in a global constraint on marine cloud feedback. This is used to update the likelihood of ECS from Sherwood et al. (2020) of 3.11 K (95% confidence: 2.26–4.70 K) to 2.86 K (95% confidence: 2.13–4.12 K). The probability of ECS above the 4.5 K upper end of the AR5 likely range becomes increasingly unlikely falling from 6.6% (Sherwood et al., 2020), to 2.3% when using constraints on global marine cloud feedback.

Our analysis points to enhanced moisture convergence in the extratropics as a key driver of enhanced cloud condensate and negative feedback in this region. The control on where moistening occurs exerted by Hadley cell expansion is found to be an important modulator of extratropical SW_{FB}. The response of cloud to moisture convergence is presented in a source-sink framework (Figure 1). Because strong sources make the extratropical atmosphere very cloudy, this results in compensation between the effects of increased moisture on cloud and increased cloud on radiation (Figure 3). The terms in Figure 3 can provide a useful process constraint for GCMs. Observations of radiative efficiency and of the response of clouds to meteorology suggest that extratropical SW_{FB} in regions of moistening is negative, albeit not as negative as predicted by many GCMs (Figure 4a). Overall,

extreme ECS is not consistent with observationally-constrained extratropical SW_{FB} when combined with other lines of evidence (Myers et al., 2021; Sherwood et al., 2020; Figure 4b and 4c).

Data Availability Statement

All CMIP data are archived at esgf-node.llnl.gov/projects/esgf-llnl/. Up-to-date ECS and cloud feedbacks are available at: https://github.com/mzelinka/cmip56_forcing_feedback_ecs or published in Zelinka et al. (2020). Output from GA7.1 using the Smith scheme are accessed through the data server at the JASMIN Centre for European Data Analysis using the Moose archive interface (https://gws-access.jasmin.ac.uk/public/mohc_shared/moose-user-doc/external_user_guide.html). The permanent access numbers are: "u-bt821", "u-bt845", "u-bt848", "u-bt850", "u-bt819", "u-bt852". MAC-LWP data can be accessed at https://disc.gsfc.nasa.gov/datasets/MACLWP_diurnal_1/summary?keywords=measures. MERRA-2 data are available at https://disc.gsfc.nasa.gov/datasets/M2TMNXSLV_5.12.4/summary?keywords=MERRA2.

Acknowledgments
DTM and PRF acknowledge support from the Process-Based Climate Simulation: Advances in High- Resolution Modelling and European Climate Risk Assessment (PRIMAVERA) project funded by the European Union's Horizon 2020 program under Grant Agreement 641727. DTM acknowledges support from the University of Wyoming. ZL and DTM acknowledge support from NASA-PMMST Grant #80NSSC22K0599. IT acknowledges support from NSERC RGPIN-2021-02720. The work of MDZ was performed under the auspices of the U.S. Department of Energy (DOE) by Lawrence Livermore National Laboratory under Contract DE-AC52-07 NA27344 and was supported by the Regional and Global Model Analysis Program of the Office of Science at the DOE. GE was supported by the APAM-GISS Co-Op (#80NSSC18M0133), NASA-TASNPP Grant #80NSSC18K1030, NASA-MAP Grant #80NSSC21K1498, DOE Grant #DE-SC0020192, and NASA-PMMST Grant #80NSSC22K0609. JM was supported by the Atmospheric System Research (ASR) program as part of the DOE Office of Biological and Environmental Research. Pacific Northwest National Laboratory is operated by Battelle Memorial Institute for the U.S. Department of Energy. MEF was supported by National Science Foundation award AWD1005319. TAM was supported in part by the NOAA Cooperative Agreement with CIRES, NA17OAR4320101, and by the NOAA/ESRL Atmospheric Science for Renewable Energy (ASRE) program. We thank two anonymous reviewers for their thoughtful comments and advice. DTM thanks Dennis Hartmann for putting forward the idea of moisture convergence as a driver of extratropical cloudiness. Data analysis was performed on JASMIN at the Centre for Environmental Data Analysis with assistance from JASMIN staff.

References

Algarra, I., Nieto, R., Ramos, A. M., Eiras-Barca, J., Trigo, R. M., & Gimeno, L. (2020). Significant increase of global anomalous moisture uptake feeding landfalling atmospheric rivers. *Nature Communications*, *11*(1), 5082. https://doi.org/10.1038/s41467-020-18876-w

Bender, F. A. M., Engström, A., Wood, R., & Charlson, R. J. (2017). Evaluation of hemispheric asymmetries in marine cloud radiative properties. *Journal of Climate*, *30*(11), 4131–4147. https://doi.org/10.1175/JCLI-D-16-0263.1

Betts, A. K., & Harshvardhan (1987). Thermodynamic constraint on the cloud liquid water feedback in climate models. *Journal of Geophysical Research*, *92*(D7), 8483–8485. https://doi.org/10.1029/JD092iD07p08483

Bjordal, J., Storelvmo, T., Alterskjær, K., & Carlsen, T. (2020). Equilibrium climate sensitivity above 5°C plausible due to state-dependent cloud feedback. *Nature Geoscience*, *13*(11), 718–721. https://doi.org/10.1038/s41561-020-00649-1

Bodas-Salcedo, A., Mulcahy, J. P., Andrews, T., Williams, K. D., Ringer, M. A., Field, P. R., & Elsaesser, G. S. (2019). Strong dependence of atmospheric feedbacks on mixed-phase microphysics and aerosol-cloud interactions in HadGEM3. *Journal of Advances in Modeling Earth Systems*, *11*(6), 1735–1758. https://doi.org/10.1029/2019ms001688

Bodas-Salcedo, A., Webb, M. J., Bony, S., Chepfer, H., Dufresne, J. L., Klein, S. A., et al. (2011). COSP: Satellite simulation software for model assessment. *Bulletin of the American Meteorological Society*, *92*(8), 1023–1043. https://doi.org/10.1175/2011BAMS2856.1

Bony, S. (2005). Marine boundary layer clouds at the heart of tropical cloud feedback uncertainties in climate models. *Geophysical Research Letters*, *32*(20). https://doi.org/10.1029/2005gl023851

Bretherton, C. S., & Blossey, P. N. (2014). Low cloud reduction in a greenhouse-warmed climate: Results from Lagrangian LES of a subtropical marine cloudiness transition. *Journal of Advances in Modeling Earth Systems*, *6*(1), 91–114. https://doi.org/10.1002/2013MS000250

Bretherton, C. S., & Caldwell, P. M. (2020). Combining emergent constraints for climate sensitivity. *Journal of Climate*, *33*(17), 7413–7430. https://doi.org/10.1175/JCLI-D-19-0911.1

Ceppi, P., Hartmann, D. L., & Webb, M. J. (2016). Mechanisms of the negative shortwave cloud feedback in middle to high latitudes. *Journal of Climate*, *29*(1), 139–157. https://doi.org/10.1175/JCLI-D-15-0327.1

Ceppi, P., McCoy, D. T., & Hartmann, D. L. (2016). Observational evidence for a negative shortwave cloud feedback in middle to high latitudes. *Geophysical Research Letters*, *43*(3), 1331–1339. https://doi.org/10.1002/2015gl067499

Ceppi, P., & Nowack, P. (2021). Observational evidence that cloud feedback amplifies global warming. *Proceedings of the National Academy of Sciences*, *118*(30), e2026290118. https://doi.org/10.1073/pnas.2026290118

Elsaesser, G. S., O'Dell, C. W., Lebsock, M. D., Bennartz, R., Greenwald, T. J., & Wentz, F. J. (2017). The multi-sensor advanced climatology of liquid water path (MAC-LWP). *Journal of Climate*, *30*(24), 10193–10210. https://doi.org/10.1175/jcli-d-16-0902.1

Field, P. R., & Heymsfield, A. J. (2015). Importance of snow to global precipitation. *Geophysical Research Letters*, *42*(21), 9512–9520. https://doi.org/10.1002/2015GL065497

Frazer, M. E., & Ming, Y. (2022). Understanding the Extratropical Liquid Water Path Feedback in Mixed-Phase Clouds with an Idealized Global Climate Model. *Journal of Climate*, 1–48. https://doi.org/10.1175/JCLI-D-21-0334.1

Frey, W. R., & Kay, J. E. (2018). The influence of extratropical cloud phase and amount feedbacks on climate sensitivity. *Climate Dynamics*, *50*(7), 3097–3116. https://doi.org/10.1007/s00382-017-3796-5

Gordon, N. D., & Klein, S. A. (2014). Low-cloud optical depth feedback in climate models. *Journal of Geophysical Research: Atmospheres*, *119*(10), 6052–6065. https://doi.org/10.1002/2013JD021052

Grise, K. M., & Medeiros, B. (2016). Understanding the varied influence of midlatitude jet position on clouds and cloud radiative effects in observations and global climate models. *Journal of Climate*, *29*(24), 9005–9025. https://doi.org/10.1175/JCLI-D-16-0295.1

Guo, Y., Shinoda, T., Guan, B., Waliser, D. E., & Chang, E. K. M. (2020). Statistical relationship between atmospheric rivers and extratropical cyclones and anticyclones. *Journal of Climate*, *33*(18), 7817–7834. https://doi.org/10.1175/JCLI-D-19-0126.1

Hall, A., & Qu, X. (2006). Using the current seasonal cycle to constrain snow albedo feedback in future climate change. *Geophysical Research Letters*, *33*(3). https://doi.org/10.1029/2005GL025127

Hartmann, D. L. (2015). *Global physical climatology* (Vol. 103). Newnes.

Held, I. M., & Soden, B. J. (2006). Robust responses of the hydrological cycle to global warming. *Journal of Climate*, *19*(21), 5686–5699. https://doi.org/10.1175/jcli3990.1

Jiang, J. H., Su, H., Zhai, C., Perun, V. S., Del Genio, A., Nazarenko, L. S., et al. (2012). Evaluation of cloud and water vapor simulations in CMIP5 climate models using NASA "A-Train" satellite observations. *Journal of Geophysical Research*, *117*(D14), D14105. https://doi.org/10.1029/2011JD017237

Kay, J. E., Medeiros, B., Hwang, Y. T., Gettelman, A., Perket, J., & Flanner, M. G. (2014). Processes controlling Southern Ocean shortwave climate feedbacks in CESM. *Geophysical Research Letters*, 2013GL058315. https://doi.org/10.1002/2013GL058315

Kelleher, M. K., & Grise, K. M. (2019). Examining Southern Ocean cloud controlling factors on daily time scales and their connections to midlatitude weather systems. *Journal of Climate*, *32*(16), 5145–5160. https://doi.org/10.1175/jcli-d-18-0840.1

Kelleher, M. K., & Grise, K. M. (2021). Varied midlatitude shortwave cloud radiative responses to Southern Hemisphere circulation shifts. *Atmospheric Science Letters*, *23*(1), e1068. https://doi.org/10.1002/asl.1068

Klein, S. A., & Hall, A. (2015). Emergent constraints for cloud feedbacks. *Current Climate Change Reports*, *1*(4), 276–287. https://doi.org/10.1007/s40641-015-0027-1

Klein, S. A., Hall, A., Norris, J. R., & Pincus, R. (2017). Low-cloud feedbacks from cloud-controlling factors: A review. *Surveys in Geophysics*, *38*(6), 1307–1329. https://doi.org/10.1007/s10712-017-9433-3

Lacis, A. A., & Hansen, J. E. (1974). Parameterization for absorption of solar-radiation in Earths atmosphere. *Journal of the Atmospheric Sciences*, *31*(1), 118–133. https://doi.org/10.1175/1520-0469(1974)031<0118:apftao>2.0.co;2

Liou, K.-N. (2002). *An introduction to atmospheric radiation*. Elsevier.

Loeb, N. G., Doelling, D. R., Wang, H., Su, W., Nguyen, C., Corbett, J. G., et al. (2018). Clouds and the earth's radiant Energy System (CERES) Energy balanced and filled (EBAF) top-of-atmosphere (TOA) edition-4.0 data product. *Journal of Climate*, *31*(2), 895–918. https://doi.org/10.1175/JCLI-D-17-0208.1

Lorenz, D. J., & DeWeaver, E. T. (2007). The response of the extratropical hydrological cycle to global warming. *Journal of Climate*, *20*(14), 3470–3484. https://doi.org/10.1175/JCLI4192.1

Lu, J., Vecchi, G. A., & Reichler, T. (2007). Expansion of the Hadley cell under global warming. *Geophysical Research Letters*, *34*(6). https://doi.org/10.1029/2006GL028443

Manaster, A., O'Dell, C. W., & Elsaesser, G. (2017). Evaluation of cloud liquid water path trends using a multidecadal record of passive microwave observations. *Journal of Climate*, *30*(15), 5871–5884. https://doi.org/10.1175/jcli-d-16-0399.1

McCoy, D. T., Field, P., Bodas-Salcedo, A., Elsaesser, G. S., & Zelinka, M. D. (2020). A regime-oriented approach to observationally constraining extratropical shortwave cloud feedbacks. *Journal of Climate*, 1–55. https://doi.org/10.1175/JCLI-D-19-0987.1

McCoy, D. T., Field, P. R., Elsaesser, G. S., Bodas-Salcedo, A., Kahn, B. H., Zelinka, M. D., et al. (2019). Cloud feedbacks in extratropical cyclones: Insight from long-term satellite data and high-resolution global simulations. *Atmospheric Chemistry and Physics*, *19*(2), 1147–1172. https://doi.org/10.5194/acp-19-1147-2019

McCoy, D. T., Field, P. R., Schmidt, A., Grosvenor, D. P., Bender, F. A. M., Shipway, B. J., et al. (2018). Aerosol midlatitude cyclone indirect effects in observations and high-resolution simulations. *Atmospheric Chemistry and Physics*, *18*(8), 5821–5846. https://doi.org/10.5194/acp-18-5821-2018

McCoy, D. T., Hartmann, D. L., & Grosvenor, D. P. (2014a). Observed Southern Ocean cloud properties and shortwave reflection. Part I: Calculation of SW flux from observed cloud properties*. *Journal of Climate*, *27*(23), 8836–8857. https://doi.org/10.1175/jcli-d-14-00287.1

McCoy, D. T., Hartmann, D. L., & Grosvenor, D. P. (2014b). Observed Southern Ocean cloud properties and shortwave reflection. Part II: Phase changes and low cloud feedback*. *Journal of Climate*, *27*(23), 8858–8868. https://doi.org/10.1175/jcli-d-14-00288.1

McCoy, D. T., Hartmann, D. L., Zelinka, M. D., Ceppi, P., & Grosvenor, D. P. (2015). Mixed-phase cloud physics and Southern Ocean cloud feedback in climate models. *Journal of Geophysical Research: Atmospheres*, *120*(18), 9539–9554. https://doi.org/10.1002/2015jd023603

Molod, A., Takacs, L., Suarez, M., & Bacmeister, J. (2015). Development of the GEOS-5 atmospheric general circulation model: Evolution from MERRA to MERRA2. *Geoscientific Model Development*, *8*(5), 1339–1356. https://doi.org/10.5194/gmd-8-1339-2015

Mulcahy, J. P., Jones, C., Sellar, A., Johnson, B., Boutle, I. A., Jones, A., et al. (2018). Improved aerosol processes and effective radiative forcing in HadGEM3 and UKESM1. *Journal of Advances in Modeling Earth Systems*, *10*(11). https://doi.org/10.1029/2018MS001464

Mülmenstädt, J., Salzmann, M., Kay, J. E., Zelinka, M. D., Ma, P.-L., Nam, C., et al. (2021). An underestimated negative cloud feedback from cloud lifetime changes. *Nature Climate Change*, *11*(6), 508–513. https://doi.org/10.1038/s41558-021-01038-1

Myers, T. A., & Norris, J. R. (2016). Reducing the uncertainty in subtropical cloud feedback. *Geophysical Research Letters*, *43*(5). https://doi.org/10.1002/2015GL067416

Myers, T. A., Scott, R. C., Zelinka, M. D., Klein, S. A., Norris, J. R., & Caldwell, P. M. (2021). Observational constraints on low cloud feedback reduce uncertainty of climate sensitivity. *Nature Climate Change*. https://doi.org/10.1038/s41558-021-01039-0

Qu, X., Hall, A., Klein, S. A., DeAngelis, & Anthony, M. (2015). Positive tropical marine low-cloud cover feedback inferred from cloud-controlling factors. *Geophysical Research Letters*. https://doi.org/10.1002/2015GL065627

Quaas, J. (2012). Evaluating the "critical relative humidity" as a measure of subgrid-scale variability of humidity in general circulation model cloud cover parameterizations using satellite data. *Journal of Geophysical Research*, *117*(D9). https://doi.org/10.1029/2012jd017495

Seager, R., & Henderson, N. (2013). Diagnostic computation of moisture budgets in the ERA-interim reanalysis with reference to analysis of CMIP-archived atmospheric model data*. *Journal of Climate*, *26*(20), 7876–7901. https://doi.org/10.1175/JCLI-D-13-00018.1

Senior, C. A., & Mitchell, J. F. B. (1993). Carbon-dioxide and climate - the impact of cloud parameterization. *Journal of Climate*, *6*(3), 393–418. https://doi.org/10.1175/1520-0442(1993)006<0393:cdacti>2.0.co;2

Sherwood, S. C., Webb, M. J., Annan, J. D., Armour, K. C., Forster, P. M., Hargreaves, J. C., et al. (2020). An assessment of Earth's climate sensitivity using multiple lines of evidence. *Reviews of Geophysics*, *58*(4), e2019RG000678. https://doi.org/10.1029/2019rg000678

Smith, R. N. B. (1990). A scheme for predicting layer clouds and their water content in a general circulation model. *Quarterly Journal of the Royal Meteorological Society*, *116*(492), 435–460. https://doi.org/10.1002/qj.49711649210

Sousa, P. M., Blamey, R. C., Reason, C. J. C., Ramos, A. M., & Trigo, R. M. (2018). The 'Day Zero' Cape Town drought and the poleward migration of moisture corridors. *Environmental Research Letters*, *13*(12), 124025. https://doi.org/10.1088/1748-9326/aaebc7

Stevens, B., & Brenguier, J. L. (2009). *Cloud controlling factors: Low clouds*. MIT Press Cambridge.

Tan, I., & Storelvmo, T. (2019). Evidence of strong contributions from mixed-phase clouds to arctic climate change. *Geophysical Research Letters*, *46*(5), 2894–2902. https://doi.org/10.1029/2018GL081871

Terai, C. R., Klein, S. A., & Zelinka, M. D. (2016). Constraining the low-cloud optical depth feedback at middle and high latitudes using satellite observations. *Journal of Geophysical Research: Atmospheres*. https://doi.org/10.1002/2016JD025233

Terai, C. R., Zhang, Y., Klein, S. A., Zelinka, M. D., Chiu, J. C., & Min, Q. (2019). Mechanisms behind the extratropical stratiform low-cloud optical depth response to temperature in ARM site observations. *Journal of Geophysical Research: Atmospheres*, *124*(4), 2127–2147. https://doi.org/10.1029/2018jd029359

Tselioudis, G., Lipat, B. R., Konsta, D., Grise, K. M., & Polvani, L. M. (2016). Midlatitude cloud shifts, their primary link to the Hadley cell, and their diverse radiative effects. *Geophysical Research Letters*, *43*(9), 4594–4601. https://doi.org/10.1002/2016GL068242

Tsushima, Y., Emori, S., Ogura, T., Kimoto, M., Webb, M. J., Williams, K. D., et al. (2006). Importance of the mixed-phase cloud distribution in the control climate for assessing the response of clouds to carbon dioxide increase: A multi-model study. *Climate Dynamics*, *27*(2–3), 113–126. https://doi.org/10.1007/s00382-006-0127-7

Tukey, J. (1958). Bias and confidence in not quite large samples. *The Annals of Mathematical Statistics*, *29*, 614. https://doi.org/10.1214/aoms/1177706635

Wentz, F. J., & Meissner, T. (2000). *AMSR ocean algorithm, version 2* (p. 66). Remote Sensing Systems.

Wielicki, B. A., Barkstrom, B. R., Harrison, E. F, Lee, R. B., III., Smith, G. L., & Cooper, J. E. (1996). Clouds and the earth's radiant Energy System (CERES): An Earth observing System experiment. *Bulletin of the American Meteorological Society*, *77*(5), 853–868. https://doi.org/10.1175/1520-0477(1996)077<0853:catere>2.0.co;2

Wilson, D. R., Bushell, A., Kerr-Munslow, A. M., Price, J. D., Morcrette, C. J., & Bodas-Salcedo, A. (2008). PC2: A prognostic cloud fraction and condensation scheme. II: Climate model simulations. *Quarterly Journal of the Royal Meteorological Society*, *134*(637), 2109–2125. https://doi.org/10.1002/qj.332

Yettella, V., & Kay, J. E. (2017). How will precipitation change in extratropical cyclones as the planet warms? Insights from a large initial condition climate model ensemble. *Climate Dynamics*, *49*(5–6), 1765–1781. https://doi.org/10.1007/s00382-016-3410-2

Zelinka, M. D., Myers, T. A., McCoy, D. T., Po-Chedley, S., Caldwell, P. M., Ceppi, P., et al. (2020). Causes of higher climate sensitivity in CMIP6 models. *Geophysical Research Letters*. https://doi.org/10.1029/2019GL085782

Zelinka, M. D., Zhou, C., & Klein, S. A. (2016). Insights from a refined decomposition of cloud feedbacks. *Geophysical Research Letters*, *43*(17), 9259–9269. https://doi.org/10.1002/2016GL069917